ELSEVIER

Biophysical Chemistry 134 (2008) 144–156

Biophysical Chemistry

http://www.elsevier.com/locate/biophyschem

Thermomyces lanuginosus lipase in the liquid-crystalline phases of aqueous phytantriol: X-ray diffraction and vibrational spectroscopic studies

Audrius Misiūnas [a,*], Zita Talaikytė [a], Gediminas Niaura [a], Valdemaras Razumas [a], Tommy Nylander [b]

[a] *Institute of Biochemistry, Mokslininkų 12, LT-08662 Vilnius, Lithuania*
[b] *Department of Physical Chemistry 1, Center for Chemistry and Chemical Engineering, P.O. Box 124, S-221 00 Lund, Sweden*

Received 25 September 2007; received in revised form 4 February 2008; accepted 6 February 2008
Available online 16 February 2008

Abstract

The influence of *Thermomyces lanuginosus* lipase (TLL) on the phase behaviour of liquid-crystalline phases of aqueous phytantriol as well as conformational changes of TLL entrapped in the cubic Q^{230} phase have been studied by small angle X-ray diffraction (SAXD), FT-Raman, and FT-IR techniques. It was found that the lipidic Q^{230} phase is able to accommodate up to 10 wt.% of TLL, and the temperature of phase transition to the inverted hexagonal phase H_{II} increases indicating stabilizing effect of the protein. FT-Raman analysis of Trp amino acid marker band W3 revealed that the average rotation angle around the C_3-C_β bond of four Trp residues of TLL in the Q^{230} phase increases. Reasoning from available TLL crystallographic data, this result is explained by structural transition of entrapped protein to so-called "open" and more related to the enzymatically-active conformation. TLL secondary structure analysis by amide I and amide III vibrational bands showed that content of α-helixes does not change, while a part of β-sheet structures transforms to less ordered elements upon incorporation of protein into the Q^{230} phase of aqueous phytantriol.

Keywords: *Thermomyces lanuginosus* lipase; Phytantriol; Aqueous liquid-crystalline phases; Small angle X-ray diffraction (SAXD); FT-IR spectroscopy; Raman spectroscopy

1. Introduction

Understanding of interaction of enzymes with lipid-like structures is of fundamental importance in order to control their biological function and construct diverse biochemical processes. It was demonstrated recently that reversed bicontinuous cubic phases are the elegant models of lipid bilayer, and provide promising approach for various technological applications [1–3]. Presence of water channel systems with diameter up to 50–100 Å separated by lipid layer provides opportunity of incorporation of various proteins and enzymes into the cubic phases [3–8]. Lipases are the enzymes functioning at the lipid/water interface activity of which dramatically depends on the microenvironment of the interface [9]. Therefore, bicontinuous cubic phases may serve as an appropriate matrix for incorporation of lipases, and analysis of their function [3,10–12].

In this work, we have studied *Thermomyces lanuginosus* lipase (TLL), an enzyme, which hydrolyzes acylglycerides (EC 3.1.1.3). TLL has a catalytic triad Ser^{146}-His^{258}-Asp^{201} [13,14] shielded from the environment by an α-helical loop or "lid" comprising of Ile^{86}-Glu^{87}-Asn^{88}-Trp^{89}-Ile^{90}-Gly^{91}-Asn^{92}-Leu^{93} residues. This enzyme is inactive in aqueous conditions but upon binding to a lipid/water interface its catalytic activity greatly enhances. The interfacial activation of lipase is associated with conformational changes of the enzyme leading to the displacement of the lid and exposing the active site [15–18]. It was established that activation of lipases critically depends on the structure of lipid/water interface. For example, TLL binds to the non-substrate small (40 nm) unilamellar vesicules of dimethyl phosphoglycerol (DMPG) in a catalytically-active form, whereas it adopts a catalytically-inactive form upon binding to zwiterionic

* Corresponding author. Tel.: +370 5 272 91 44; fax: +370 5 272 9196.
E-mail address: audriusm@bchi.lt (A. Misiūnas).

0301-4622/$ - see front matter © 2008 Elsevier B.V. All rights reserved.
doi:10.1016/j.bpc.2008.02.002

dimethyl phosphocholine (DMPC) or to a large (100 nm) DMPG vesicles [19–21]. TLL undergoes conformational transition upon specific interactions with anionic micelles of sodium taurodeoxycholate and mixed micelles of sodium taurodeoxycholate/phosphatidylcholine, resulting in the changes of microenvironment of the Trp^{89} residue [22]. Moreover, it was demonstrated that hydrolysis of triolein catalyzed by lipase from *Rhisopus delemar* in AOT [sodium bis(2-ethylhexyl)sulfosuccinate] reverse micelle systems with alkanes is influenced by the degree of curvature of micelle interface [23].

Vibrational spectroscopy is able to provide detailed molecular picture of the enzyme structure and conformational changes due to its function [24]. For lipases, important molecular-level information on activation mechanism is expected to be acquired from vibrational spectra. However, applications of vibrational spectroscopic technique are not abundant [25–28], in part, because of the complexity of the lipid/water interface required for the function of lipases. Thus, Natalello et al. [25] has determined the secondary structure content of *Candida rugosa* lipase by FT-IR spectroscopy analysis of the amide I band absorption in H_2O and D_2O solutions. Good agreement between X-ray data and vibrational spectroscopy was emphasized. Moreover, in addition to X-ray data, FT-IR method predicted the existence of two classes of α-helical structures. Comparative FT-IR spectroscopic studies of lipases from *Candida antarctica* B and *Pseudomonas cepacia* in aqueous solution, and in the solid state (dehydrated form) revealed decreased the α-helix and increased the β-sheet content upon lyophilization of the enzymes [26]. In this work, the amide III spectral region was employed for secondary structure analysis. It was suggested that, in the FT-IR studies of solid proteins, the method overestimates the β-sheet content by measuring other hydrogen bonded structures.

Several works were devoted to spectroscopic monitoring of adsorption at interface induced structural changes in lipases [27,29,30]. Noinville et al. [27] have studied in-situ the secondary structure changes of TLL adsorbed on the hydrophobic surface (Si coated with octadecyltrichlorsilane) by attenuated total reflection FT-IR technique. In contrast to other studied proteins (bovine serum albumin, lysozyme, and α-chymotrypsin), no changes in secondary structure was detected for TLL at the first stage of adsorption, while slight increase in the content of β-structures was observed at monolayer coverage. Based on the H/D exchange experiments, it was concluded that, at the interface, TLL adopts an enzymatically-active, "open" conformation. Near-UV circular dichroism (CD) spectroscopy studies have revealed an increase in β-sheet content upon incorporation of *Rhizopus arrhizus* lipase into the reverse micelles [29]. However, for the same lipase bound to dipalmitoyl phosphatidylcholine (DPPC) vesicles, a slight increase in the α-helical content was determined [30].

The purpose of the present work is to investigate the environmental effects and structural changes of TLL arising from the interaction with an interface of liquid-crystalline structures formed by aqueous 3,7,11,15-tetramethyl-1,2,3-hexadecanetriol (phytantriol; Phyt), giving particular attention to the enzyme state in the Phyt-based bicontinuous cubic phases. Phyt is a neutral polar lipid well-known as ingredient in cosmetics (Fig. 1). Phase

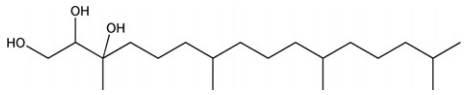

Fig. 1. Structural formula of 3,7,11,15-tetramethyl-1,2,3-haxanetriol (phytantriol).

behaviour of the Phyt/H_2O system [31] is similar to that of monooleoyl glycerol which is commonly used for the preparation of cubic liquid-crystalline phases with different surface curvatures [32–37]. However, liquid-crystalline structures of monooleoyl glycerol, due to the presence of ester linkage, are hydrolyzed by lipase [10–12]. By changing Phyt/water ratio and/or temperature, it is possible to obtain lamellar L_α, cubic Q^{230} or Q^{224}, and reversed hexagonal H_{II} liquid-crystalline phases [31]. At first, the influence of TLL incorporation on the phase behaviour of Phyt/H_2O system was studied by small angle X-ray diffraction measurements (SAXD). Interaction of TLL with Phyt bilayer and enzyme backbone secondary structure changes were probed by FT-Raman and FT-IR spectroscopies. To the best of our knowledge, up to now, no reports on FT-Raman studies of TLL were published.

2. Experimental

2.1. Materials and sample preparation

3,7,11,15-Tetramethyl-1,2,3-hexadecanetriol (phytantriol, Phyt) was obtained from Aldrich, and used without additional purification. *T. lanuginosus* lipase (TLL) solution (batch #:110 K1357, Sigma) was dialyzed against 5 mM phosphate buffer (pH 7.5), the solution was concentrated by ultra-filtration, and lyophilized. Water was distilled and passed through a Milli-Q water purification system (Millipore S.A., Molsheim). Phyt-based liquid-crystalline phases were prepared as follows. Appropriate amounts of TLL lyophilised powder were dissolved in water and added to the vials with weighted amounts of Phyt. According to the phase diagram published in [31], the Phyt/water weight ratios were kept at 90/10 (lamellar phase), 78/22 and 73/27 (Q^{230} and Q^{224} cubic phases, respectively), and 74/26 (hexagonal phase). Final amounts of TLL in the samples were 0.1, 0.5, 1.0, 2.0, 5.0 and 10.0 wt.%. The vials were immediately sealed and centrifuged up and down at 2000 g for 30 min. This operation was repeated several times.

2.2. Small angle X-ray diffraction (SAXD) measurements

Small angle X-ray diffraction measurements were performed on a Kratky compact small-angles system equipped with an OED 50 M position-sensitive detector (MBraun, Graz, Austria) containing 1024 channels of 53.1 μm width. Cu K_α nickel-filtered radiation of 1.542-Å wavelength was provided by Seifert ID 3000 X-ray generator (Rich Seifert, Ahresburg, Germany) operating at 55 kV and 40 mA. A few milligrams of sample was put between thin mica windows in a steel sample holder. Temperature was controlled within ±0.1 °C by using a Peltier element. Measurements were carried out in the temperature

range from 25 to 65 °C with increment of 5 °C in heating. Samples were equilibrated at appropriate measurement temperature for 15 min. X-Ray data were evaluated using a 3D-View software (MBraun, Graz, Austria).

2.3. FT-Raman and FT-IR spectroscopic measurements

Raman spectroscopic measurements were carried out with Perkin–Elmer Model Spectrum GX FT-Raman spectrometer equipped with an InGaAs detector operating at room temperature. An air-cooled diode-pumped Nd-YAG laser provided the excitation with emission wavelength of 1064 nm. In general, the laser power at the sample was 300 mW. The spectral resolution was set at 4 cm^{-1}, and the wavenumber increment per data point was 1 cm^{-1}. In order to enhance the signal-to-noise ratio, approximately 1000–4000 scans were co-added. Samples of liquid-crystalline phases were placed into holder for powder and sealed with a thin glass window. Solvent spectra were normalized according to the buffer bands and digitally subtracted from the protein solution spectra. For the studies of TLL in Q^{230} phase, the spectrum of pure phase (without an enzyme) was normalized according to the Phyt peak at 1149 cm^{-1} and subtracted from the spectrum of protein-containing liquid-crystalline phase.

FT-IR spectra were recorded with the same Perkin–Elmer Model Spectrum GX FT-IR spectrometer equipped with DTGS detector. The spectral resolution was set to 4 cm^{-1}, and all of the spectra were acquired by 500 scans. Solutions were measured in CaF_2 cells, samples of liquid-crystalline phases were compacted between ZnSe windows, solid TLL was pressed with KBr to obtain pellets. Solvent spectra were normalized according to the association band of water at 2125 cm^{-1} and subtracted from the protein-containing sample spectra [38].

2.4. Amide I and amide III band fitting

For amide I band analysis, the extended frequency region (1580–1720 cm^{-1}) of FT-Raman spectrum was chosen to account for the contribution of aromatic amino acid residues on the parameters of amide group vibrations [39]. The spectral region below 1630 cm^{-1} was fitted by 5–6 relatively narrow, with full width at half maximum (FWHM) of 5–12 cm^{-1}, components representing vibrations of Trp, Phe, and Tyr residues, while amide vibrational contour (1630–1720 cm^{-1}) was fitted by five component bands assigned to α-helix (1652–1655 cm^{-1}), organized β-sheet (1669–1672 cm^{-1}), strongly hydrogen bonded disordered (1630–1645 cm^{-1}), and two non-hydrogen bonded disordered (1680–1693 and 1696–1702 cm^{-1}) secondary structures [39–44]. The high-frequency disordered structure components might incorporate vibrations of loose β-strands and polyproline II (PPII) structural elements [39], while the low-frequency (strongly hydrogen-bonded) disordered structure component might have the contribution from the vibronic coupling modes [39,45]. The FWHM of the components varied from 10 to 21 cm^{-1}. Spectra were fitted with Gaussian form components.

The amide III vibrational region of FT-IR spectra was fitted by Gaussian components number and position of which were determined from the second derivatives of the experimental profile [46]. The peak positions of the components were allowed to vary within 2 cm^{-1} from initial values during fitting procedure. The components within frequency region of 1295–1330 cm^{-1} were assigned to α-helix, 1220–1250 cm^{-1} — to β-sheet, and 1250–1295 cm^{-1} — to the disordered secondary structure elements (β-turns, random coils, and loose strands) [46,47].

The contents of TLL secondary structure elements were estimated from the assigned components as fractional areas of the total area in the amide I and amide III frequency regions. Fitting was performed by using GRAMS AI software assuming linear baseline. The standard error for intense peak frequencies was found to be 1–2 cm^{-1}, and for the FWHM values — 2–4 cm^{-1}. The standard error for area estimates was within 10% of calculated value.

3. Results and discussion

3.1. Phase behaviour of Phyt/H_2O system containing TLL

Previously [31], it has been demonstrated that, depending on water content, at room temperature Phyt forms lamellar L_α, Q^{230} cubic of *Ia3d* symmetry, and Q^{224} cubic of *Pn3m* symmetry liquid-crystalline phases. Reversed hexagonal H_{II} phase is observed only at elevated temperatures (40–60 °C). Replacement of a part of Phyt by TLL results in the transformations of liquid-crystalline phases depending on the content of entrapped enzyme (Fig. 2). Small amounts of TLL (<0.5 wt.%) do not perturb the structure of the liquid-crystalline phases, while larger quantities induce decrease of the lattice parameter a_0 or phase transition. For instance, the entrapment of >5 wt.% TTL in the L_α phase leads to the planar bilayer alterations and phase transition from L_α to inverted micelles (L_2). The same quantities of TLL at 45 °C transform H_{II} phase to L_2 phase. Why the Q^{230} phase accommodates the highest content of TLL? In the binary Phyt/H_2O system [31], as in the celebrated monoolein/H_2O system [32], there is conclusive experimental evidence for the presence of a body-centered structure of *Ia3d* symmetry at lower

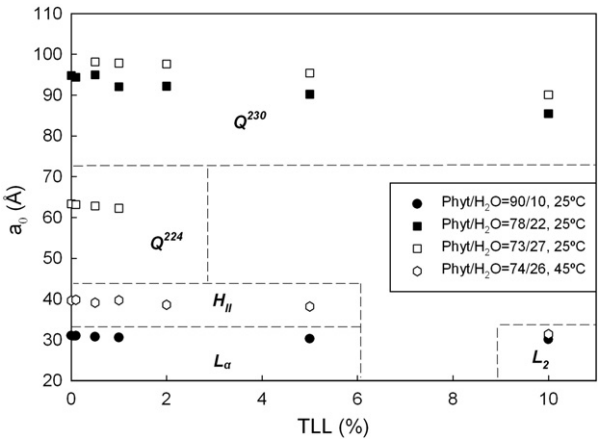

Fig. 2. Influence of TLL amount on the lattice parameter a_0 of lamellar (triangles) (Phyt/H_2O=90/10 weight ratio), hexagonal (hexagones) (Phyt/H_2O=76/24 weight ratio), Q^{230} (black squares) (Phyt/H_2O=78/22 weight ratio) and Q^{224} (white squares) (Phyt/H_2O=73/27 weight ratio) liquid-crystalline phases. Dashed lines divide different phases.

water content, and of the primitive cubic phase of symmetry *Pn3m* at higher water content. This finding agrees with relative phase locations well; the bilayer transforms from the *Ia3d* phase to the *Pn3m* phase upon dilution [33]. Different alternative structures, *Im3m*, *Pn3m*, and *Ia3d* form in the ternary lipid/protein/water systems [4,34]. However, the *Ia3d* structure, compared to the *Im3m* and *Pn3m* structures, contains no circular necks. The phase forms straight helical tubes oriented parallel to the four (111) directions of the unit cell, and the absolute value of the surface-averaged Gaussian curvature is highest in the Q^{230} phase. It has been shown by Andersson et al. [35] that increased surface curvature might be responsible for the increased force of absorption.

As can be seen from Fig. 2, the process goes opposite to above discussed situation, Q^{224} cubic phase is able to accommodate less than 0.5 wt.% of TLL, while at 0.5 and 1 wt.% TLL concentration the mixture of Q^{224} and Q^{230} phases is detected, which transforms to the pure Q^{230} phase at higher amounts of TLL (2–10 wt.%). Contrary to the Q^{224} phase, the Q^{230} phase of Phyt/H_2O system is able to accumulate considerably larger quantities of TLL (up to 10 wt.%) without the formation of other liquid-crystalline structures. The only effect of the presence of TLL in this phase is the decrease of a_0 value (Δa_0=9 Å at 10 wt.% of TLL). The proposed model is based on the possibility of forming section of a cubic lipid-water phase which gives a two-dimensional minimal surface (*Ia2d*) with "holes" facing alternate sides of the bilayer. If these holes through the bilayer are plugged with protein molecules, we can form a bilayer that is closely related to the "planar" bilayer conformation [36,37].

The structure of liquid-crystalline phases transforms upon heating. The magnitude of thermal vibrations of the hydrocarbon chain atoms increases with temperature. The bonds in the sheets formed by the polar head groups are strong compared to the weak van der Waals interactions between adjacent chains. Hence, in a certain temperature range, the chains become fluid while the polar groups are still associated in to the sheets. The overall structure then comprises lipid bilayers with disordered chains. Fig. 3 shows the action of temperature on the phase behaviour of aqueous Phyt containing different amounts of TLL. The lipid bilayer thickness decreases with the linear temperature increment. For the L_α phases (Phyt/H_2O=90/10 system), the temperature of $L_\alpha \rightarrow L_2$ phase transition significantly decreases with increasing TLL quantity (Fig. 3a). It should be noted that the phase containing 10 wt.% of TLL (L_2 phase) converts to liquid unordered lipid–protein mixture already at about 30 °C. It follows that the entrapment of TLL into the L_α phase of Phyt/H_2O system induces destruction of the planar lipid bilayer. Contrary to the L_α phase, in the case of Q^{230} phase with Phyt/H_2O mixture of 78/22 weight ratio, the $Q^{230} \rightarrow H_{II}$ phase transition temperature gradually increases with the increase of TLL content (Fig. 3b). For this cubic phase with 10 wt.% of TLL, the transition temperature increase (ΔT) was found to be ca. 5 °C. Again, this can be explained by formation of the two-dimensional minimal surface with the "holes" facing alternate sides of the bilayer, and the incorporated proteins protects from the fast destruction of the *Ia3d*

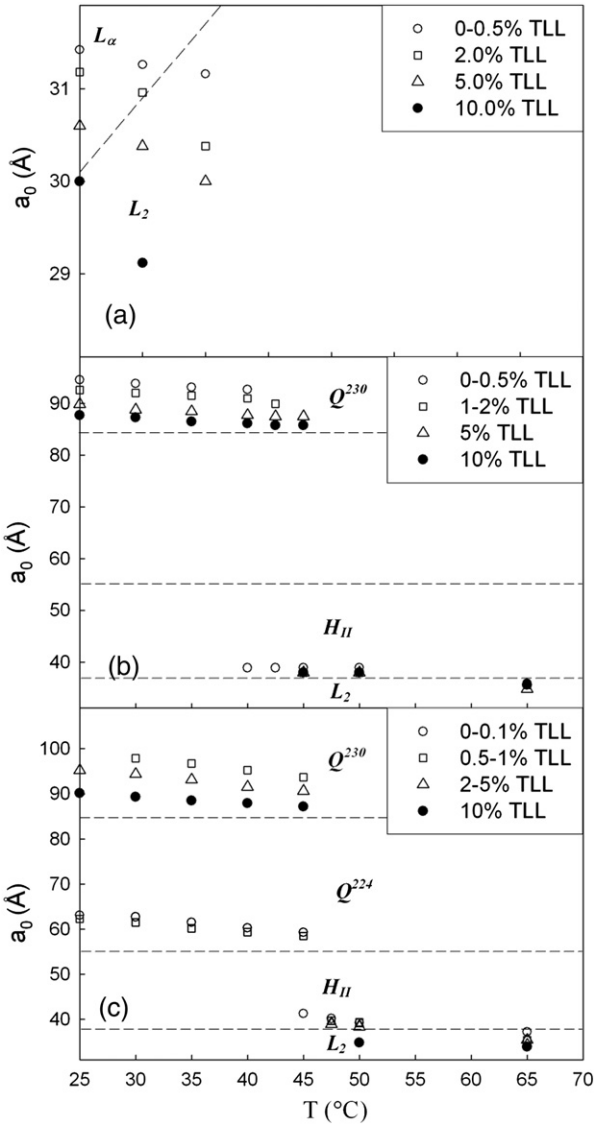

Fig. 3. Influence of temperature on the lamellar (a), Q^{230} (b) and Q^{224} (c) liquid-crystalline phases of Phyt/TLL/H_2O system. Dashed lines divide different phases.

phase. Similar temperature effect is observed for the Phyt/H_2O=73/27 system (Fig. 3c). At low TLL concentrations and up to 45 °C, pure Q^{224} phase is detected which, with increasing protein content, transforms to the mixture of $Q^{224}+Q^{230}$ phases (0.5–1 wt.% of TLL), pure Q^{230} phase (2–5 wt.% of TLL), and finally to the H_{II} phase. At the 0.5–5 wt.% content of TLL, the transition temperature is found to be higher by ca. 2.5 °C as compared to the Phyt/H_2O system without TLL [31]. The Q^{230} phase of this system with 10 wt.% of TLL transforms directly to the L_2 phase at ca. 50 °C. Increase of the phase transition temperature of the above-mentioned cubic phase evidences that presence of TLL stabilizes this liquid-crystalline structure.

Thus, based on SAXD findings we are able to conclude that incorporation of TLL into the Phyt/H_2O system promotes formation and stabilization of the Q^{230} cubic phase of *Ia3d* symmetry and destabilization of lamellar phase. The Q^{230} cubic phase demonstrates a broad interval of thermal stability and can accommodate considerable amounts of enzyme.

3.2. Structural changes of TLL entrapped in the Q^{230} phase of aqueous Phyt as studied by FT-Raman and FT-IR spectroscopies

Considering the results of foregoing section, the Q^{230} phase of Phyt was selected for further spectroscopic investigation of TLL interactions with Phyt/H_2O interface. FT-Raman and FT-IR spectroscopic techniques are sensitive to the protein secondary structure and conformational changes of particular amino acid residues [24,39,40]. Raman spectroscopy was used for the evaluation of the structural and environmental features of aromatic amino acid residues and for protein backbone conformations, while FT-IR spectroscopy was a supplementary method for the study of TLL secondary structure.

Fig. 4 compares the FT-Raman spectra of Phyt-based Q^{230} cubic phase containing 10 wt.% of TLL (Fig. 4a) and without the enzyme (Fig. 4b). Both spectra are dominated by the intense features of Phyt matrix. Recently, based on the OH/OD isotopic substitution, molecular modelling, measurements of polarized Raman spectra, and temperature-dependent spectral changes, we have assigned the Phyt vibrational modes, and have evaluated the hydrogen bonding and interchain interaction marker bands [48]. The most intense doublet at 1439 and 1460 cm^{-1} belongs to bending vibrations of CH_2/CH_3 groups. Methylene wagging and twisting modes are visible at 1336 and 1305 cm^{-1}, while peaks in the vicinity of 1149, 1055, and 735 cm^{-1} correspond to C − C stretching vibrations [48]. The broad peak near 813 cm^{-1} belongs to rocking vibrations of CH_2/CH_3 group. It is suggested that this mode might be employed for hydrogen bonding interaction studies. To extract vibrational modes of enzyme entrapped into the liquid-crystalline cubic phase, we constructed difference spectrum (Fig. 4c) by subtracting the spectrum of pure Q^{230} phase (Fig. 4b) from that of the phase containing TLL (Fig. 4a). Regardless the presence of very intense Raman peaks of Phyt, difference spectrum clearly exhibits features characteristic for non-resonant Raman spectra of proteins [40].

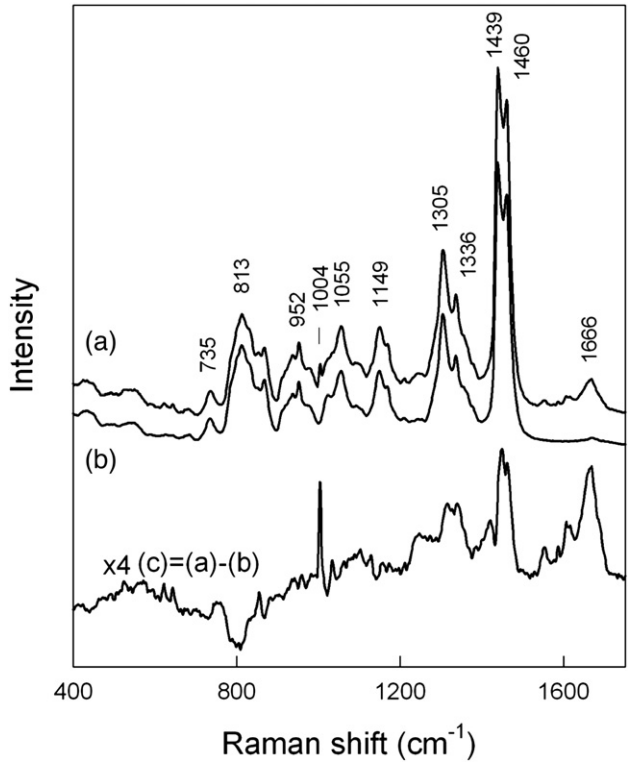

Fig. 4. FT-Raman spectra of Phyt/TLL/H_2O=70/10/20 (weight ratio) liquid-crystalline Q^{230} cubic phase (a), Phyt/H_2O=80/20 liquid-crystalline Q^{230} cubic phase (b), and difference spectrum (c) = (a)–(b). Spectra are normalized according to the 1149 cm^{-1} peak of phytantriol. The excitation wavelength is 1064 nm, 4000 scans are co-added.

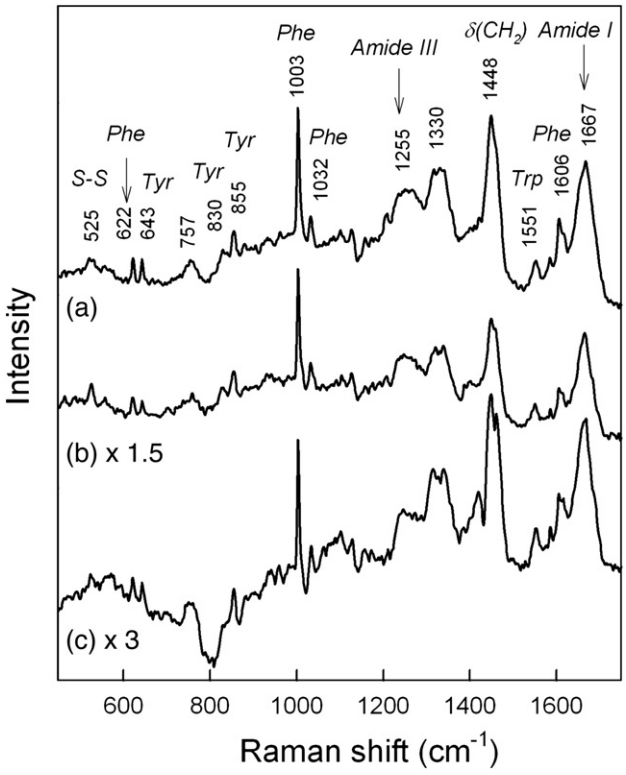

Fig. 5. FT-Raman spectra of TLL in solid state (a), in 20 mM phosphate buffer of pH 7.5 (b), and in Phyt/TLL/H_2O=70/10/20 (weight ratio) liquid-crystalline Q^{230} cubic phase (c) The excitation wavelength is 1064 nm, 1000 scans were co-added for solid TLL, and 4000 scans for solution and cubic phase spectra.

Fig. 5 compares the FT-Raman spectra of TLL in different environments, and Table 1 summarizes vibrational modes and provides the assignments of the bands based on previous protein Raman spectroscopic studies [39–42,49–58]. To the best of our knowledge, Raman spectrum of this enzyme was not described in the literature.

The spectra of Fig. 5 are dominated from contributions of aromatic amino acid residues and amide vibrational modes. The band frequencies assigned to the different vibrations of amino acid residues are the averaged frequencies of individual residues, while their FWHMs reflects differences in the band positions of individual groups. TLL contains 15 Phe, 10 Tyr, and 4 Trp residues. Accordingly, the most intense peak in the spectrum at 1003 cm^{-1} corresponds to well-defined totally symmetric ring breathing vibrational mode of Phe residues [42,55]. Parameters of this mode are not sensitive to the environmental changes, and thus 1003-cm^{-1} peak may serve as

Table 1
Tentative assignments of TLL Raman bands for solid protein sample (lyophilized powder), dissolved in 20 mM phosphate buffer (pH 7.5), and incorporated in the Q^{230} cubic phase of aqueous Phyt

Solid	20 mM PB (pH 7.5)	Q^{230} cubic phase	Assignment
520 m	525 m	524 m	ν(S−S)
556 w	558 w	557 w, br?	Amide VI
622 m	621 m	621 m	Phe
643 m	643 m	643 m	Tyr
756 m, br	758 m, br	757 m, br	Trp, Ala
829 w	828 w	829 m	Tyr
855 m	855 m	855 m	Tyr
880 vw	880 w	880 w	Trp
933 w	931 w	935 w	ν(C−C)
962 m	959 w	959 m	δ(CCC), $\rho_s(CH_3)$, $\rho_s(CH_2)$, ν(C−Ca)
1004 vs	1004 vs	1004 vs	Phe
1032 m	1032 m	1033 m	Phe
1101 w	1104 w	1102 w	ν(C−C), ν(C−N), ν(C−O)
1127 m	1127 m	1127 m	ν(C−C), ν(C−N)
1158 w	1158 w	1157 m	ν(C−C), ν(C−N)
1172 vw	1175 w	1172 w	$t(CH_2)$, $\rho(CH_3)$, Tyr
1208 w	1207 w	1211 w	Tyr, Phe
1255	1252	1249	Amide III
1317 s	1321 s	1315 s	Amide III, $t(CH_2)$, w(CH_2)
1331 s	1331 s	1327 s	Amide III, $\delta(CH_2)$
1341 s	1339 s	1338 s	Trp, $\delta(CH_2)$
~1357 sh		~1357 sh	Trp
	1388 vw	1385 w	$\nu_s(COO^-)$
1401 vw	1400 vw	1400 sh	$\nu_s(COO^-)$
1421 w	1426 w	1420 m	$\delta(CH_2)$
1449 vs	1449 vs	1449 vs	$\delta(CH_2)$
1458 vs, sh	1458 vs, sh	1462 vs	$\delta(CH_2)$, $\delta(CH_3)$
1552 m	1550 m	1553 m	Trp
1585 w	1586 w	1586 w	Phe
1606 m	1606 m	1606 m	Phe
1615 m, sh	1613 m, sh	1616 m	Tyr
1667 vs	1665 vs	1664 vs	amide I
2879 s	2878 s	2878 s	$\nu(CH_2)$
2936 vs	2936 vs	2939 vs	$\nu(CH_3)$, $\nu(CH_2)$
2967 sh	2967 sh	2969 sh	$\nu_{as}(CH_3)$
3061 m	3065 m	3062 m	ν(=C−H) aromatic

Abbreviations: PB, phosphate buffer; vs, very strong; m, medium; w, weak, vw, very weak; sh, shoulder; br, broad; ν, stretching; δ, deformation; ρ, rocking; ρ_s, symmetric rocking; t, twisting; w, wagging.

an intensity standard in concentrational analysis or evaluation of relative intensities in Raman spectra [42,55]. Other Phe peaks are located at 622, 1032, 1586, and 1606 cm^{-1} (Fig. 5, Table 1).

3.2.1. Tryptophan side chain markers

Contrary to Phe, parameters of vibrational modes of Trp residues are sensitive to conformation, hydrogen bonding interaction, and hydrophobicity of the environment surrounding the indole ring. Consequently, useful spectrum-structure correlations have been established [49–54]. The well-defined and intense pyrrole ring band near 1550 cm^{-1} was found to be localized to C_2=C_3 bond (Fig. 6) stretching motion (labelled W3), and it was demonstrated that this mode is sensitive to the conformation of tryptophan residues [49]. Because W3 mode involves vibration of C_3 atom, its frequency depends on the torsion angle $\chi^{2,1}$ about the $C_2C_3-C_\beta C_\alpha$ moiety (rotation around the $C_\beta-C_3$ bond) in accordance with the following relationship [50,52]:

$$\nu(\mathrm{W3}) = 1542 + 6.7\left(\cos 3|\chi^{2,1}| + 1\right)^{1.2} \quad (1)$$

Comparison of the TLL spectrum in the Q^{230} phase with the spectrum in aqueous phosphate buffer (PB) solution (Fig. 6) reveals obvious spectral changes in the position of Trp band. The frequency of the ν(W3) band of TLL in the cubic phase increases by 3 cm^{-1}, while the position of Phe bands remains unshifted. Such frequency shift is clearly visible in the difference spectrum (Fig. 6c) as derivative form feature in the vicinity of 1540–1560 cm^{-1}. Considering the ν(W3) band as a marker for the average $|\chi^{2,1}|$ angle of the four Trp residues in TLL, we have found by using Eq. (1) that the entrapment

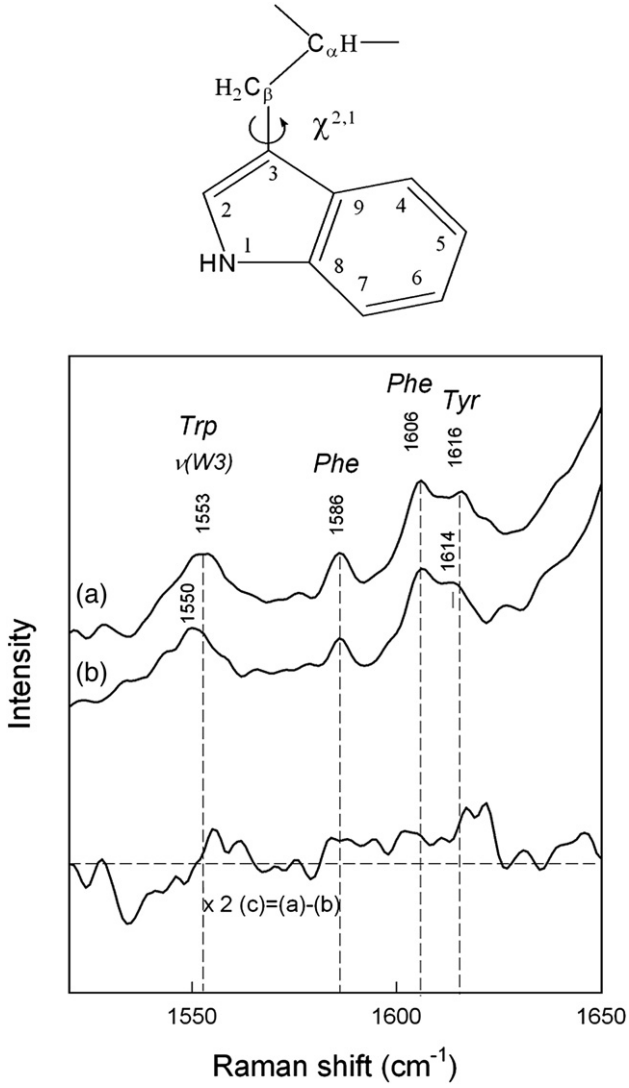

Fig. 6. Structure and atom numbering for Trp residue, and FT-Raman spectra in 1520–1650 cm^{-1} range of TLL in Phyt/TLL/H_2O=70/10/20 (weight ratio) liquid-crystalline Q^{230} cubic phase (a), and 20 mM phosphate buffer solution of pH 7.5 (b). Difference spectrum (c)=(a)–(b) is also shown. The excitation wavelength is 1064 nm, 4000 scans are co-added.

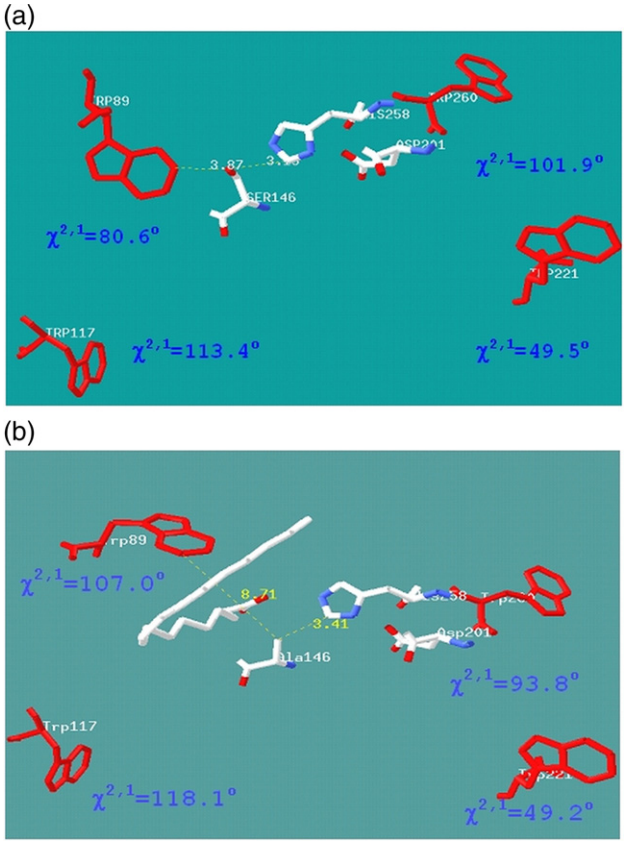

Fig. 7. Active centres of the wild-type TLL ("closed" form; PDB ID 1DT3), and of the complex of TLL(S146A) mutant with oleic acid ("opened" form; PDB ID 1GT6).

of TLL into the Q^{230} phase results in increase of the $|\chi^{2,1}|$ value from 95°±2° to 103°±2°. Being average value of four Trp residues, the *ν*(W3) band is broadened for TLL in both Q^{230} phase (FWHM = 16.2 cm^{-1}) and PB solution (FWHM = 15.0 cm^{-1}) as compared with L-tryptophan in water solution (FWHM = 12.0 cm^{-1}) or in the crystalline phase (FWHM = 12 ± 1 cm^{-1}) [53] implying the different values of $|\chi^{2,1}|$ for the individual Trp residues in TLL. It is of interest to compare the obtained $|\chi^{2,1}|$ angle values with the averaged values calculated from the crystallographic data of TLL given in Protein Data Bank (PDB). Fig. 7a displays the orientation of four Trp residues and the active centre triad, comprising Ser^{146}, His^{258} and Asp^{201} residues [13,14], for the wild-type TLL molecule in the closed inactive form. Fig. 7b shows the same four Trp residues and the Ala^{146}-His^{258}-Asp^{201} triad of mutated TLL with trapped oleic acid to afford opened enzyme conformation. The calculations show that for wild-type TLL in Fig. 7a, which exists in enzymatically-inactive closed conformation, the averaged $|\chi^{2,1}|$ value equals to 86.4°, whereas for the complex of TLL(S146A) mutant with oleic acid (Fig. 7b), existing in the enzymatically-active opened conformation, the averaged $|\chi^{2,1}|$ angle increases to 92.0°. Noteworthy, comparing both models, one can see that the major changes of the rotation angles of discrete Trp residues occur near the catalytic centre (Trp^{260} and especially Trp^{89} of the lid). Thus, spectroscopically observed increase of $|\chi^{2,1}|$ is in accordance with the assumption that, in the Q^{230} phase, TLL takes conformation close to the opened one.

Other important marker bands of Trp side chains are the doublet in the vicinity of 1340–1373 cm^{-1}, arising from the Fermi resonance between the fundamental in-plane $N_1 - C_8$ stretch (mode W7) and combination bands of the ring out-of-plane vibrations [50,54]. It was demonstrated that the intensity ratio of high to low-frequency doublet components depends on the hydrophobicity of the environment of indole ring, increasing for more hydrophobic environment [50,51,54]. Fig. 8 compares the spectra of TLL in the Q^{230} phase and PB solution in the W7 doublet frequency region. In the non-resonant Raman spectra of proteins, the low-frequency component of the doublet at ~1340 cm^{-1} is overlapped with the CH vibration of aliphatic chains and intensity of the high-frequency component at ~1360 cm^{-1}, rather than the intensity ratio can be employed as the marker of hydrophobic interaction strength of indole ring [51]. Thus, increase of the 1360-cm^{-1} band intensity reflects increase in hydrophobicity of the environment. In the spectrum of TLL entrapped in the Q^{230} phase (Fig. 8a), the high-frequency component of W7 doublet at 1358 cm^{-1} is much stronger than the corresponding band of enzyme in the PB solution (Fig. 8b), indicating that an averaged Trp residue of TLL in the cubic phase are located in more hydrophobic microenvironment than in the PB solution.

Thus, analysis of the W3 and W7 bands in the FT-Raman spectra suggests that Trp residues of TLL in the Q^{230} phase are located in more hydrophobic environment compared with PB solution, and their averaged rotation angle $|\chi^{2,1}|$ around the $C_3 - C_\beta$ bond increases. These observations imply that TLL in the Phyt-based phase undergoes structural transformation which results in an open-like and more related to the enzymatically-active conformation of the protein.

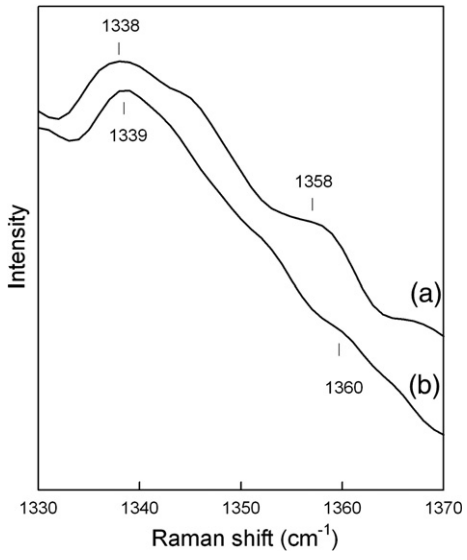

Fig. 8. Fermi resonance doublet of Trp in FT-Raman spectra of TLL in the Phyt-based Q^{230} phase (a) and 20 mM phosphate buffer solution of pH 7.5 (b). The excitation wavelength is 1064 nm, 4000 scans are co-added.

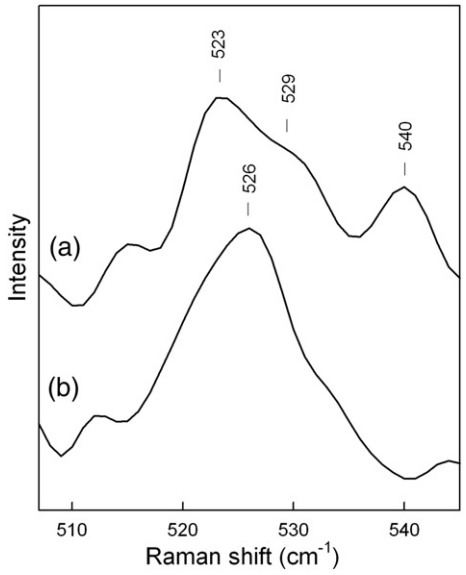

Fig. 9. Bands of S − S stretching vibrations in the FT-Raman spectra of TLL in the Q^{230} phase (a), and 20 mM phosphate buffer solution of pH 7.5 (b). The excitation wavelength is 1064 nm, 4000 scans are co-added.

3.2.2. Disulfide stretching bands

Conformation of three disulfide bridges present in TLL also can be sensitively probed by Raman spectroscopy. Previous studies with model compounds revealed correlation between the S − S stretching frequency, ν(S − S), and conformation of backbone C − CH_2 − S − S − CH_2 − C fragments [56–58]. Fig. 9 shows the TLL spectra in the Q^{230} phase and PB solution in the S − S stretching frequency region. It is evident that the moderate intensity peak at 526 cm^{-1} observed in the TLL solution spectrum (Fig. 9b) splits into the three components located at 523, 529, and 540 cm^{-1} (Fig. 9a) upon entrapment of enzyme into the Q^{230} cubic phase. Since it was shown previously [56–58] that the 525-cm^{-1} band is characteristic for the *trans-gauche-gauche* rotamers of C − CH_2 − S − S − CH_2 − C fragment, presence of single and well-defined peak at 526 cm^{-1} for TLL in PB solution suggest that backbone conformation around all of the disulfide bridges is similar, i.e. *trans-gauche-gauche*. However, entrapment of TLL into the Q^{230} phase results in dramatic conformational changes around one of the S − S bridges, from *trans-gauche-gauche* to *trans-gauche-trans*, because of appearance of diagnostic high-frequency ν(S − S) peak at 540 cm^{-1} [57,58]. It seems that conformation around the other two S − S bridges also changes slightly. Presence of two peaks at 523 and 529 cm^{-1} (Fig. 9a) indicates distortions within the dihedral angles of C − CH_2 − S − S − CH_2 − C moieties. Thus, spectroscopic data of Fig. 9 clearly demonstrate that interaction of TLL with Phyt/H_2O interface influences the conformation of backbone C − CH_2 − S − S − CH_2-C fragments.

Recent crystallographic study [59] suggests that isomerization of the Cys^{268} − Cys^{22} disulfide is one of the key structural factors accompanying the transition of TLL from "low activity" form to "activated" form. In this light, presented Raman spectroscopic evidence on the conformation changes around the S − S bridges supports our assumption of TLL active centre "opening" upon incorporation into the Phyt-based cubic Q^{230} phase.

3.2.3. Amide vibrational bands

For the TLL secondary structure studies, we have employed the amide I and amide III bands in FT-Raman and FT-IR spectra, respectively. Amide I band (1620–1695 cm^{-1}) has an appreciable Raman intensity and is observed in the spectral region free from Phyt scattering (Fig. 4). The main contribution for amide I mode comes from the backbone C=O stretching motion (83%) coupled with an out-of-phase C − N stretching and C − C − N deformation [41]. Frequency of C=O stretching mode depends on the strength of hydrogen bonding interaction involving the amide group and dipole–dipole interaction between the carboxyl groups, making the amide I mode sensitive to the organization of amide linkages [24]. Fig. 10 compares the FT-Raman spectra of TLL in the Q^{230} phase and PB solution in the extended amide I frequency region (1580–1720 cm^{-1}). The spectral range below 1620 cm^{-1} is dominated by the ring vibrations of aromatic amino acid residues, while frequency window between 1620 and 1720 cm^{-1} is dominated by the amide I vibrations [39]. The spectral contours are complex indicating presence of different conformational backbone structures. Based on literature data [39–44], we have attributed the main three secondary structure elements to the following frequency intervals: an α-helical structures at 1650–1660 cm^{-1}, organized β-sheet structures at 1670–1675 cm^{-1}, and disordered structures (including β-turns, loose β-strands, and polyproline II structures) at 1680–1690 cm^{-1}. The lower frequency components in the spectral range of 1630–1645 cm^{-1} we tentatively attributed to strongly

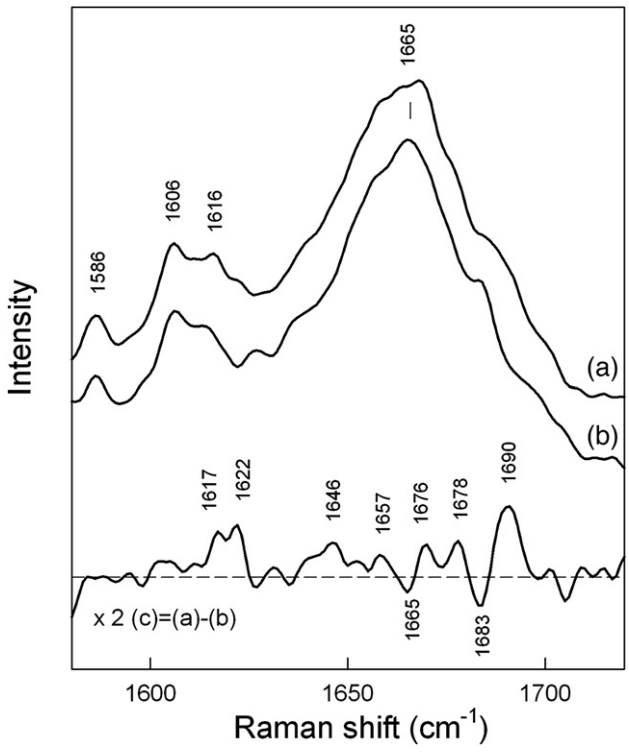

Fig. 10. FT-Raman spectra of TLL in the amide I region: TLL in the Phyt-based Q^{230} cubic liquid-crystalline phase (a), TLL in 20 mM phosphate buffer of pH 7.5 (b), difference spectrum (c). The spectra of pure Q^{230} phase and buffer were subtracted. The excitation wavelength is 1064 nm, 4000 scans were co-added. The spectra are normalized according to the intensity of Phe peak at 1003 cm^{-1}.

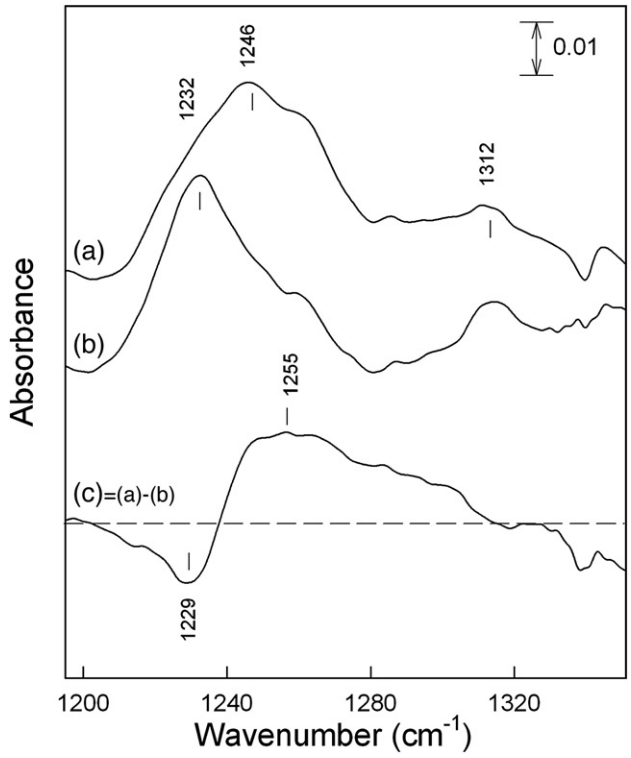

Fig. 11. FT-IR spectra of TLL in the amide III region: TLL in the Phyt-based Q^{230} cubic liquid-crystalline phase (a), TLL in 20 mM phosphate buffer of pH 7.5 (b), difference spectrum (c). The spectra of pure Q^{230} phase and buffer solution were subtracted.

hydrogen bonded β-sheet structures [24]. Let us consider the difference spectrum, which probes most directly the changes in secondary structure of TLL in different environments (Fig. 10c). The most pronounced perturbations are visible in the 1680–1695 cm^{-1} frequency range. Appearance of derivative-like feature with negative-going and positive-going branches at 1683 and 1690 cm^{-1}, respectively, suggests the decrease in hydrogen bonding strength of unorganized secondary structures of TLL in the Q^{230} phase [24]. It is evident that the positive-going 1690-cm^{-1} peak is relatively intense, which is consistent with increasing the number of unorganized amide groups. The positive-going peaks at 1617 and 1622 cm^{-1} reflects perturbations in the structure and state of Tyr and Trp side chains, respectively.

Additional information on the perturbation in secondary structure of TLL was obtained from the analysis of amide III region of FT-IR spectra (Fig. 11). The main contribution for amide III mode comes from the N − H in-plane bending (52%) vibration coupled with in-phase C − N stretching (14%), C − C stretching (18%), and C=O in-plane bending vibrations [41]. In spite of the fact that intensity of amide III band is about 5–10 fold weaker as compared with amide I band [47], it has important advantages due to the absence of H_2O interference and better resolved positions of various secondary structure elements [46,47,60]. For our study, it is important that amide III mode falls into the spectral range where absorption of Phyt is relatively weak. Based on previous investigations [46,47], we have assigned the bands in amide III region to the following secondary structure elements: 1295–1330 cm^{-1}, α-helix; 1220–1250 cm^{-1}, β-sheet; and 1250–1295 cm^{-1}, disordered structures (including β-turns, loose β-strands, and polyproline II structures). Amide III band in FT-IR spectrum of entrapped TLL differs from the corresponding mode in PB solution (Fig. 11). The bandwidth of the mode increases and peak maximum shifts towards higher wavenumbers. Difference spectrum (Fig. 11c) clearly shows increase in population of disordered structures (1255-cm^{-1} positive-going peak) and decrease of β-sheet (1229-cm^{-1} negative-going peak) secondary structures for TLL in the Phyt-based Q^{230} phase.

For more quantitative analysis of the relative changes of TLL secondary structure due to the entrapment into the Q^{230} phase, the experimental curves were resolved into the Gaussian components number of which was determined from the second derivatives of the experimental profile (Fig. 12). Table 2 summarizes the parameters of the components constituting the amide I and amide III spectral contours. The extended amide I spectral region (Fig. 12a,b) at the low-frequency side contains components due to aromatic amino acid residues (1580–1630 cm^{-1}) included in the fitting procedure to account for the contribution to the parameters of the amide components. Five components assigned to different secondary structure elements (Table 2) were required for fitting the amide I spectral contour in the frequency region 1630–1720 cm^{-1}, while 8–9 components were necessary for amide III range (1220–1330 cm^{-1}). Some of the amide III components are relatively narrow (7–9 cm^{-1}) and may have a contribution from side chain amino acid vibrations. Examination of the fitting results shows that the most intense bands for both spectral regions correspond to organized β-sheet structures, intensity of which decreases upon entrapment of TLL into the Q^{230} phase. However, the intensity of main

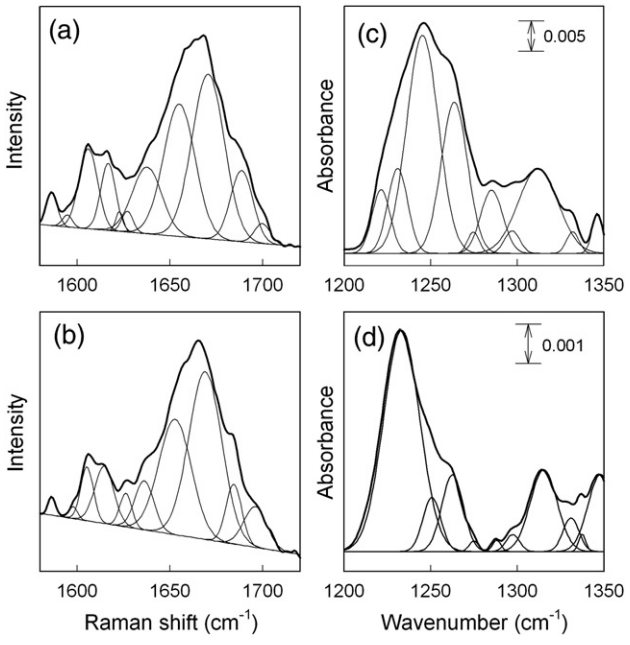

Fig. 12. Amide I Raman (a, b) and amide III FT-IR (c, d) bands of TLL in the Phyt-based Q^{230} phase (a, c) and in 20 mM phosphate buffer of pH 7.5 (b, d) with added Gaussian curve fitting.

Table 2
Curve fitting parameters[a] of amide I and amide III bands for TLL in 20 mM phosphate buffer (pH 7.5) and entrapped into the Q^{230} cubic phase of aqueous Phyt

Secondary structure	TLL in phosphate buffer			TLL in cubic Q^{230} phase		
	Band position (cm^{-1})	FWHM (cm^{-1})	Area (%)	Band position (cm^{-1})	FWHM (cm^{-1})	Area (%)
FT-Raman amide I band						
α-helix	1653	21	31	1655	20	31
Organized β-sheet	1669	21	46	1671	21	40
Disordered (including weakly-hydrogen bonded, loose β-strand, PPII)	1684	10	8	1689	14	12
Strongly-hydrogen bonded structure, vibronic coupled modes	1696	14	7	1700	10	2
	1636	12	8	1638	19	15
FT-IR amide III band						
α-helix				1297	10	2
	1315	18	16	1312	27	18
	1331	11	4	1332	8	1
Organized β-sheet				1221	12	6
	1233	25	58	1231	14	9
				1245	21	35
Disordered (including β-turns,	1251	12	7			
loose β-strands, PPII)	1263	15	12	1264	18	21
	1275	7	1	1275	8	1
	1288	6	1	1285	15	7
	1297	9	1			

[a] Standard errors for peak positions and FWHM values are 1–2 and 2–4 cm^{-1}, respectively. The standard error for area estimates is within 10% of calculated value.

α-helix components in both FT-Raman (1653–1655 cm^{-1}) and FT-IR spectra (1312–1315 cm^{-1}) does not change significantly. Several components were attributed to disordered secondary structures. The low-frequency amide I Raman components around 1636–1638 cm^{-1} (Table 2) are, most likely, due to strongly hydrogen bonded C=O groups [39,45]. It was suggested also that the band near 1630 cm^{-1} results from strong transition dipole coupling in antiparallel-chain sheet structure [45]. Even though such assignment seems to be appropriate for infrared studies [24], the relatively high scattering efficiency from disordered structures was recently pointed out by Sane et al. [39] for Raman band near 1641 cm^{-1}. Thus, we tentatively assigned the FT-Raman components around 1636–1638 cm^{-1} due to strongly hydrogen bonded disordered secondary structures. Intensity of this low-frequency component clearly increases for TLL in the Q^{230} phase as compared with buffer solution (Fig. 12, Table 2). On the high-frequency side of the FT-Raman spectrum two components in the frequency region of 1684–1700 cm^{-1} we attributed to vibration of weakly hydrogen bonded less ordered secondary structures than α-helix or β-sheet. Interestingly, the frequency of these two components further increases (from 1684 and 1696 cm^{-1} to 1689 and 1700 cm^{-1}, respectively) (Table 2), indicative of decrease in the strength of hydrogen bonding interaction of TLL C=O groups in the Q^{230} phase. The assignment of disordered structures in the amide III region of FT-IR spectra is rather obvious [46,47]. The typical example is the component near 1263–1264 cm^{-1}. Again, intensity of this band clearly increases upon entrapment of TLL into the Q^{230} phase (Table 2).

Table 3
Fractional band areas (A) of peptide chain conformations of TLL in 20 mM phosphate buffer (pH 7.5), and entrapped into the Q^{230} cubic phase determined from amide I and amide III bands of FT-Raman and FT-IR spectra, respectively, and area ratios for various conformations

TLL state	Fractional band areas of peptide chain conformations (%)			$A_{(\alpha\text{-helix})}/A_{(\beta\text{-sheet})}$	$A_{(disord)}/A_{(\beta\text{-sheet})}$
	α-helix	Organized β-sheet	Disordered[a]		
From FT-Raman amide I band					
PB solution	31	46	23	0.67	0.50
Q^{230} phase	31	40	29	0.78	0.73
From FT-IR amide III band					
PB solution	20	58	22	0.34	0.38
Q^{230}	21	50	29	0.42	0.58

Abbreviations: PB, phosphate buffer.
[a] Areas of several components were co-added (see Table 2).

For more obvious analysis of secondary structure changes of TLL, we have calculated the relative amounts of different secondary structure elements as fraction areas of the total amide I and amide III contour area (Table 3). The content of α-helixes determined by FT-Raman method (31%) is close to the helix content (33% for α- and 3_{10}-helixes) estimated by X-ray crystallography [17]. However, it should be noted that absolute content of the protein secondary structure cannot be evaluated from the vibrational spectrum because of difference in intrinsic intensities for particular structures. The strength of vibrational spectroscopy is in the ability to assess the relative differences in secondary structure [24] induced, in our case, by TLL transfer from pure PB solution into the Q^{230} phase. Examination of Table 3 shows several important tendencies. First of all, the relative content of α-helixes as compared with organized β-sheets ($A_{(\alpha\text{-helix})}/A_{(\beta\text{-sheet})}$) increases for TLL in the Q^{230} phase. Such

changes are associated with decrease in population of β-sheet structures. Secondly, the relative content of disordered structures, as compared with β-sheet elements ($A_{(disord)}/A_{(\beta\text{-sheet})}$), markedly increases. It should be pointed out that the tendencies obtained from the analysis of amide I band, at least semi-quantitatively, are consistent with that obtained from amide III contour. Our analysis suggests that a part of organized β-sheet structures transforms to less ordered secondary structure elements upon incorporation of TLL into the Phyt-based cubic phase.

Previous infrared spectroscopic studies have demonstrated minor perturbations in secondary structure of small (12.4 kDa) water-soluble protein cytochrome *c* entrapped into the Q^{230} cubic phase of monoolein [5]. The estimated content of protein secondary structures was found to be similar for solution and cubic phase. However, decrease in unfolding temperature by 4 °C was established for protein incorporated in the monoolein-based phase. More defined structural destabilization and aggregation was detected for larger (25.8 kDa) protein α-chymotrypsin entrapped into the cubic phase of monoolein [8]. FT-IR spectroscopic measurements of amide I' mode have indicated increase in random coil content characteristic for aggregated protein. Infrared spectroscopic studies of adsorbed proteins have demonstrated that, in general, interaction of proteins with hydrophobic surfaces induces greater conformational changes to less ordered secondary structures as compared to hydrophilic surfaces [61]. Decrease in α-helix and increase in β-sheet/random structures were clearly detected upon adsorption of bovine serum albumin and fibrinogen on a CH_3-terminated surface, while considerably less disordering was estimated for the HO-terminated (hydrophilic) surfaces [61]. It has been shown that drop in adsorbed lysozyme activity correlates with the loss of α-helical content [62]. Noinville et al. [27] have studied the conformation and solvation changes of TLL adsorbed at hydrophobic surface using attenuated total reflection FT-IR spectroscopy. Contrary to bovine serum albumin, lysozyme, and α-chymotrypsin, no secondary structure changes were detected at first stage of TLL adsorption, and only a slight folding of β-structures was observed for the complete enzyme monolayer. It was suggested that TLL adopts open conformation at water/hydrophobic surface interface. As in the case for adsorbed TLL [27], secondary structure analysis presented in this work shows stability of the α-helix content indicating general integrity of the protein in Phyt-based Q^{230} phase. Observed rearrangement of β-sheet structures, leading to the increase in unordered (including β-turns, loose β-strands, and PPII) elements, points to the conformational changes of the entrapped enzyme. Taking into account the above discussion of FT-Raman data on the perturbations in geometry of Trp residues and S − S bridges, we suggest that, upon entrapment into the Q^{230} phase, TLL adopts new conformation, possibly more "open"-like. Open conformation differs from the closed form (characteristic for TLL in PB solution) by larger hydrophobic domain exposed to the enzyme surface [15]. Such protein conformation at the Phyt/H_2O interface might cause stabilization of the Phyt-based cubic phases which, in our SAXD data, shows up as increase in the $Q^{230} \rightarrow H_{II}$ (Fig. 3b) and $Q^{224} \rightarrow L_2$ (Fig. 3c) transition temperatures. As already noted, the *Ia3d* structure, compared to other two celebrated *Im3m* and *Pn3m* structures, contains no circular necks, the phase forms straight helical tubes oriented parallel to the four (111) directions of the unit cell, and the absolute value of the surface-averaged Gaussian curvature is highest in the Q^{230} phase. It has been shown by Andersson et al. [35] that increased surface curvature might be responsible for the increased force of absorption. Thus, the open-like structure of TLL might be most "visible", namely, in the *Ia3d* phase of aqueous Phyt, although thus far more proof of this statement is needed.

4. Conclusions

We have probed the structure and entrapment of triglyceride hydrolase (EC 3.1.1.3) *T. lanuginosus* lipase (TLL) into liquid-crystalline phases of aqueous phytantriol (Phyt) by small angle X-ray diffraction (SAXD) and vibrational spectroscopy techniques. SAXD data revealed that small amounts of TLL (<0.5 wt%) do not perturb the structure of liquid-crystalline phases, while larger protein amounts induce reduction of the lattice parameter (a_0) or leads to phase transitions. As the TLL concentration in lamellar L_α phase increases (>5 wt.%), a phase transition to the inverted micelle L_2 phase takes place. Temperature-dependent experiments reveal marked lowering of the $L_\alpha \rightarrow L_2$ transition temperature in the presence of protein as compared with pure lamellar phase of Phyt/H_2O, implying that incorporation of TLL promotes the destruction of planar Phyt bilayer. SAXD measurements indicate that at 25 °C the bicontinuous Q^{224} cubic phase can accommodate only up to 0.5 wt.% of TLL, and the phase transforms to the Q^{230} phase at higher protein content. It has been found that the Q^{230}cubic phase is able to accommodate up to 10 wt.% of the protein. This protein-containing phase transforms to the reversal hexagonal structure H_{II} at higher temperature (by ca. 5 °C) indicating stabilization of the Q^{230} phase by protein.

The changes in conformation of amino acid side chains and secondary structure of TLL incorporated into the Phyt-based Q^{230} phase as compared with phosphate buffer solution were probed by FT-Raman and FT-IR spectroscopies. Analysis of tryptophan Raman marker bands W7 and W3 revealed that, on average, the four Trp residues of TLL incorporated in the phase are located in more hydrophobic environment when compared to phosphate buffer, and their average rotation angle $|\chi^{2,1}|$ around the $C_3 - C_\beta$ bond increases. Such geometric changes were found to be in accord with crystallographic data for transition of the "closed" TLL form to the "opened" conformation. Thus, our spectroscopic observations suggest that, in the Phyt-based Q^{230} cubic phase, TLL takes an "open"-like and more related to the enzymatically-active conformation. FT-Raman data exposed distinct conformational changes within $C - CH_2 - S - S - CH_2 - C$ fragments due to the entrapment of TLL into the Q^{230} phase. Disulfide bridge frequencies showed that conformation around one of the three S − S bridges undergoes transition from *trans-gauche-gauche* to *trans-gauche-trans*.

Secondary structure analysis of TLL amide I and amide III bands by FT-Raman and FT-IR techniques, respectively, revealed similar tendencies. It was found that content of α-helix structures does not change, while a part of β-sheet structures transforms to less ordered (disordered) elements upon incorporation of protein into the cubic phase. Spectroscopic data suggest that

reorganization of β-sheet secondary structure of TLL at the Phyt/H_2O interface might be responsible for the stabilization of the Q^{230} phase, as revealed by thermotropic SAXD measurements.

Acknowledgement

Financial support from the European Community under contract NMP4-CT-2003-505211 is gratefully acknowledged.

References

[1] K. Larsson, Cubic lipid-water phases: structures and biomembrane aspects, J. Phys. Chem. 93 (1989) 7304–7314.
[2] E.M. Landau, J.P. Rosenbusch, Lipidic cubic phases: a novel concept for the crystallization of membrane proteins, Proc. Natl. Acad. Sci. U. S. A. 93 (1996) 14532–14535.
[3] V. Razumas, in: M.L. Lynch, P.T. Spicer (Eds.), Bicontinuous cubic phases of lipids with entrapped proteins: structural features and bioanalytical applications, Bicontinuous liquid crystals, Surfactant science series, vol. 127, Taylor & Francis, Roca Baton, 2005, p. 169.
[4] V. Razumas, K. Larsson, Y. Miezis, T. Nylander, A cubic monoolein cytochrome *c* water phase: X-ray diffraction, FT-IR, differential scanning calorimetric, and electrochemical studies, J. Phys. Chem. 100 (1996) 11766–11774.
[5] J. Lendermann, R. Winter, Interaction of cytochrome *c* with cubic monoolein mesophases at limited hydration conditions: the effects of concentration, temperature and pressure, Phys. Chem. Chem. Phys. 5 (2003) 1440–1450.
[6] J. Barauskas, V. Razumas, T. Nylander, Entrapment of glucose oxidase into the cubic Q^{230} and Q^{224} phases of aqueous monoolein, Prog. Colloid & Polym. Sci. 116 (2000) 16–20.
[7] S.B. Leslie, S. Puvvada, B.R. Ratna, A.S. Rudolph, Encapsulation of hemoglobin in a bicontinuous cubic phase lipid, Biophys. Biochim. Acta. — Biomembranes 1285 (1996) 246–254.
[8] J. Kraineva, C. Nicolini, P. Thiyagarajan, E. Kondrashkina, R. Winter, Incorporation of α-chymotrypsin into the 3D channels of bicontinuous cubic lipid mesophases, Biochim. Biophys. Acta 1764 (2006) 424–433.
[9] R.D. Schmid, R. Verger, Lipases: interfacial enzymes with attractive applications, Angew. Chem., Int. Ed. Engl. 37 (1998) 1608–1633.
[10] R. Wallin, T. Arnebrant, The activity of lipase at the cubic liquid-crystalline phase water interface, J. Colloid Interface Sci. 164 (1994) 16–20.
[11] J. Borne, T. Nylander, A. Ehan, Effect of lipase on different lipid liquid crystalline phases formed by oleic acid based acylglycerols in aqueous systems, Langmuir 18 (2002) 8972–8981.
[12] J. Borne, T. Nylander, A. Khan, Effect of lipase on monoolein-based cubic phase dispersion (cubosomes) and vesicles, J. Phys. Chem., B 106 (2002) 10492–10500.
[13] A. Svendsen, Lipase protein engineering, Biochim. Biophys. Acta 1543 (2000) 223–238.
[14] L. Brady, A.M. Brzozowski, Z.S. Derewenda, E. Dodson, G. Dodson, S. Tolley, J.P. Turkenburg, L. Christiansen, B. Huge-Jensen, L. Norskov, L. Thim, U. Menge, A serine protease triad forms the catalytic center of a triacylglycerol lipase, Nature 343 (1990) 767–770.
[15] U. Derewenda, L. Swenson, Y.Y. Wei, R. Green, P.M. Kobos, R. Joerger, M.J. Haas, Z.S. Derewenda, Conformational lability of lipases observed in the absence of an oil–water interface. Crystallographic studies of enzymes from the fungi *Humicola lanuginosa* and *Rhisopus delemar*, J. Lipid Res. 35 (1994) 524–534.
[16] A.M. Brzozowski, U. Derewenda, Z.S. Derewenda, G.G. Dodson, D.M. Lawson, J.P. Turkenburg, F. Bjorkling, B. Huge-Jensen, S.A. Patkar, L. Thim, A model for interfacial activation in lipases from the structure of a fungal lipase-inhibitor complex, Nature 351 (1991) 491–494.
[17] D.M. Lawson, A.M. Brzozowski, S. Rety, C. Verma, G.G. Dodson, Probing the nature of substrate binding in *Humicola lanuginosa* lipase through X-ray crystallography and intuitive modelling, Protein Eng. 7 (1994) 543–550.
[18] A. Jutila, K. Zhu, Sh.A. Patkar, J. Vind, A. Svendsen, P.K.J. Kinnunen, Detergent-induced conformational changes of *Humicola lanuginosa* lipase studied by fluorescence spectroscopy, Biophys. J. 78 (2000) 1634–1642.
[19] Y. Cajal, M.A. Busquets, H. Carvajal, V. Girona, M.A. Alsina, Effects of a fungal lipase on membrane organization evaluated by fluorescence polarization, J. Mol. Catal., B Enzym. 22 (2003) 315–328.
[20] Y. Cajal, A. Svendsen, J. De Bolos, S.A. Patkar, M.A. Alsina, Effect of the lipid interface on the catalytic activity and spectroscopic properties of a fungal lipase, Biochimie 82 (2000) 1053–1061.
[21] Y. Cajal, A. Svendsen, V. Girona, Sh.A. Patkar, M.A. Alsina, Interfacial control of lid opening in *Thermomyces lanuginosa* lipase, Biochemistry 39 (2000) 413–423.
[22] A. Stobiecka, The conformational changes of the fungal lipase from *Humicola lanuginosa* induced by the formation of bile salt and mixed micelles, J. Fluoresc. 10 (2000) 307–315.
[23] K. Naoe, S. Awatsu, Y. Yamada, M. Kawagoe, K. Nagayama, M. Imai, Solvent condition in triolein hydrolysis using AOT reverse micellar system, Biochem. Eng. J. 18 (2004) 49–55.
[24] M. Jackson, H.H. Mantsch, The use and misuse of FTIR spectroscopy in the determination of protein structure, Crit. Rev. Biochem. Mol. Biol. 30 (1995) 95–120.
[25] A. Natalello, D. Ami, S. Brocca, M. Lotti, S.M. Doglia, Secondary structure, conformational stability and glycosylation of a recombinant *Candida rugosa* lipase studied by Fourier-transform infrared spectroscopy, Biochem. J. 385 (2005) 511–517.
[26] G. Vecchio, F. Zambianchi, P. Zacchetti, Fourier-transform infrared spectroscopy study of dehydrated lipases from *Candida antarctica* B and *Pseudomonas cepacia*, Biotechnol. Bioeng. 64 (1999) 545–551.
[27] S. Noinville, M. Revault, M.H. Baron, A. Tiss, S. Yapoudijan, M. Ivanova, R. Verger, Conformational changes and orientation of *Humicola lanuginosa* lipase on a solid hydrophobic surface: in situ interface Fourier transform infrared-attenuated total reflection study, Biophys. J. 82 (2002) 2709–2719.
[28] E. Horvūth, J. Gajūri, J. Kristżf, ħ. Rũdey, L. Kocsis, Monitoring of enzyme catalysed reactions by Fourier transform Raman spectrometry, Anal. Chim. Acta 370 (1998) 191–197.
[29] E.D. Brown, R.Y. Yada, A.G. Marangoni, The dependence of the lipolytic activity of *Rhizopus arrhizus* lipase on surfactant concentration in Aerosol-OT/isooctane reverse micelles and its relationship to enzyme structure, BBA-Prot. Struct. Mol. Enzymol. 1161 (1993) 66–72.
[30] A.G. Marangoni, Studies on the interaction of *Rhisopus arrizus* lipase with dipalmitoylphosphatidylcholine liposomes, Colloids and Surfaces B, Biointerfaces 1 (1993) 167–176.
[31] J. Barauskas, T. Landh, Phase behavior of the phytantriol/water system, Langmuir 19 (2003) 9562–9565.
[32] K. Larson, Two cubic phases in monoolein–water system, Nature 304 (1983) 664.
[33] S.T. Hyde, S. Andersson, B. Ericsson, K. Larsson, A cubic structure consisting of a lipid bilayer forming an infinite periodic minimal surface of the gyroid type in the glycerolmonooleate water system, Z. Kristallogr. 168 (1984) 213–219.
[34] B. Ericsson, K. Larsson, K. Fontell, A cubic protein–monoolein–water phase, Biochim. Biophys. Acta 729 (1983) 23–27.
[35] S. Andersson, S.T. Hyde, K. Larsson, S. Lidin, Minimal surfaces and structures: from inorganic and metal crystals to cell membranes and biopolymers, Chem. Rev. 88 (1988) 221–242.
[36] K. Larsson, S. Andersson, Bonnet transformation of infinite periodic minimal surfaces with hexagonal symmetry, Acta Chem. Scand. B40 (1986) 1–27.
[37] S.T. Hyde, S. Andersson, K. Larsson, Differential geometry of a model membrane consisting of a lipid bilayer with a regular array of protein units, Z. Kristallogr. 174 (1986) 237–245.
[38] F. Dousseau, M. Therrien, M. Pézolet, On the spectral subtraction of water from the FT-IR spectra of aqueous solutions of proteins, Appl. Spectrosc. 43 (1989) 538–542.
[39] S.U. Sane, S.M. Cramer, T.M. Przybycien, A holistic approach to protein secondary structure characterization using amide I band Raman spectroscopy, Anal. Biochem. 269 (1999) 255–272.

[40] R. Tuma, Raman spectroscopy of proteins: from peptides to large assemblies, J. Raman Spectrosc. 36 (2005) 307–319.
[41] S. Krimm, J. Bandekar, Vibrational spectroscopy and conformation of peptides, polypeptides, and proteins, Adv. Protein Chem. 38 (1986) 181–364.
[42] G. Niaura, in: R.A. Meyers (Ed.), Encyclopedia of Analytical Chemistry, Raman spectroscopy in analysis of biomolecules, John Wiley & Sons Ltd., Chichester, 2000, pp. 623–654.
[43] A. Torreggiani, G. Fini, Drug-antiserum molecular interactions: a Raman spectroscopic study, J. Raman Spectrosc. 30 (1999) 295–300.
[44] K. Huang, N.C. Maiti, N.B. Phillips, P.R. Carey and M.A. Weiss, Biochemistry 45 (2006) 10278–10293.
[45] S. Krimm, A. Yasuaki, Intermolecular interaction effects in the amide I vibrations of beta polypeptides, Proc. Natl. Acad. Sci. U. S. A. 69 (1972) 2788–2792.
[46] F.-N. Fu, D.B. DeOliveira, W.R. Trumble, H.K. Sarkar, B.R. Singh, Secondary structure estimation of proteins using amide III region of Fourier transform infrared spectroscopy: application to analyse calcium-binding-induced structural changes in calsequestrin, Appl. Spectroc. 48 (1994) 1432–1441.
[47] Sh. Cai, B.R. Singh, Identification of b-turn and random coil amide III infrared bands for secondary structure estimation of proteins, Biophys. Chem. 80 (1999) 7–20.
[48] A. Misiūnas, G. Niaura, Z. Talaikytė, O. Eicher-Lorka, V. Razumas, Infrared and Raman bands of phytantriol as markers of hydrogen bonding and interchain interaction, Spectrochim. Acta, A 62 (2005) 945–957.
[49] T. Miura, H. Takeuchi, I. Harada, Tryptophan Raman bands sensitive to hydrogen bonding and side-chain conformation, J. Raman Spectrosc. 20 (1989) 667–671.
[50] H. Takeuchi, Raman structural markers of tryptophan and histidine side chains in proteins, Biopolymers (Biospectroscopy) 72 (2003) 305–317.
[51] T. Miura, H. Takeuchi, I. Harada, Characterization of individual tryptophan side chains in proteins using Raman Spectroscopy and hydrogen-deuterium exchange kinetics, Biochemistry 27 (1988) 88–94.
[52] T. Miura, H. Takeuchi, I. Harada, Characterization of tryptophan side chains in lysozyme bound to inhibitors: role of the hydrophobic box in the enzymatic function, Biochemistry 30 (1991) 6074–6080.
[53] H. Takeuchi, Y. Nemoto, I. Harada, Environments and conformations of tryptophan side chains of Gramicidin A in phospholipid bilayers studied by Raman spectroscopy, Biochemistry 29 (1990) 1572–1579.
[54] I. Harada, T. Miura, H. Takeuchi, Origin of the doublet at 1360 and 1340 cm^{-1} in the Raman spectra of tryptophan and related compounds, Spectrochim. Acta, A 42 (1986) 307–312.
[55] W.B. Fischer, H.H. Eysel, Polarized Raman spectra and intensities of aromatic amino acid phenylalanine, tyrosine and tryptophan, Spectrochim. Acta, A 48 (1992) 725–732.
[56] H. Sugeta, A. Go, T. Miyazawa, Vibrational spectra and molecular conformations of dialkyl disulfides, Bull. Chem. Soc. Jpn. 46 (1973) 3407–3411.
[57] H.E. Van Wart, H.A. Scheraga, Agreement with the disulfide stretching frequency-conformation correlation of Sugeta, Go, and Miyazawa, Proc. Natl. Acad. Sci. U. S. A. 83 (1986) 3064–3067.
[58] D.M. Byler, H. Susi, H.M. Farrell Jr., Laser-Raman spectra, sulfhydryl groups and conformation of cystine linkages of b-lactoglobulin, Biopolymers 22 (1983) 2507–2511.
[59] A.M. Brzozowski, H. Savage, C.S. Verma, J.P. Turkenburg, D.M. Lawson, A. Svendsen, S. Patkar, Structural origins of the interfacial activation in *Thermomyces* (*Humicola*) *lanuginosa* lipase, Biochemistry 39 (2000) 15071–15082.
[60] K. Griebenow, A.K. Klibanov, Lyophilization-induced reversible changes in the secondary structure of proteins, Proc. Natl. Acad. Sci. U. S. A. 92 (1995) 10969–10976.
[61] P. Roach, D. Farrar, C.C. Perry, Interpretation of protein adsorption: surface-induced conformational changes, J. Am. Chem. Soc. 127 (2005) 8168–8173.
[62] A. Sethuraman, G. Belfort, Protein structural perturbation and aggregation on homogeneous surfaces, Biophys. J. 88 (2005) 1322–1333.